Available online at www.sciencedirect.com
ScienceDirect
Trans. Nonferrous Met. Soc. China 33(2023) 2646−2659
Transactions of Nonferrous Metals Society of China
www.tnmsc.cn

High-throughput exploration of composition-dependent elasto-plastic and diffusion properties of refractory multi-element Ti−Nb−Zr−W alloys

Zhu-hao WEN[1], Hao-qin LIN[1], Wei-min CHEN[1], Kewu BAI[2], Li-jun ZHANG[3]

1. Institute of Advanced Wear & Corrosion Resistant and Functional Materials, Jinan University, Guangzhou 510632, China;
2. Institute of High Performance Computing, Agency for Science, Technology and Research, Singapore 138632, Singapore;
3. State Key Laboratory of Powder Metallurgy, Central South University, Changsha 410083, China

Received 6 April 2022; accepted 11 July 2022

Abstract: A combinatorial material synthesis and analysis method can offer a great promise of mapping the elasto-plastic and diffusion properties in refractory multi-element alloys of Ti−Nb−Zr−W system with various compositions. Six groups of Ti−Nb−Zr−W quaternary diffusion couples annealed at 1273 K for 25 h were prepared and measured by electron probe microanalysis and nanoindentation tests. Subsequently, the composition-dependent elasto-plastic properties in a wide composition range of Ti−Nb−Zr−W system were obtained by using two analytical methods including Oliver−Pharr analysis and reverse analysis algorithms. Moreover, elasto-plastic property and interdiffusion coefficient databanks of BCC Ti−Nb−Zr−W system were established by using the machine learning and pragmatic numerical inverse methods, respectively. A hot workability parameter defined by the ratio of Young's modulus to main interdiffusion coefficient was proposed to evaluate the behavior during the hot working. Finally, wear resistance of refractory multi-element alloys was also discussed and verified by the experimental results. The results reveal that Ti-rich refractory multi-element alloys with the low W content have high hardness, good wear resistance, high stress, and excellent processability during the hot working, while the relatively high W content cannot improve the elasto-plastic properties of Ti-rich refractory alloys.

Key words: elasto-plastic property; interdiffusion coefficient; Ti−Nb−Zr−W alloy; diffusion couple; nanoindentation

1 Introduction

Refractory multi-element alloys are attracting more and more attention due to exceptional elasto-plastic properties [1−3]. The recently designed refractory multi-principal element alloys have good room temperature and elevated temperature elasto-plastic properties and oxidation resistance, which can be utilized as promising alloys with optimum integrated properties for aerospace and aircraft applications [4−6]. Due to the low density of element Ti, Ti-rich refractory alloys with the body-centered cubic (BCC) structure have rather lower densities compared to other refractory alloys, and have potential for development into newly low-density refractory alloys. Moreover, Ti–Nb–Zr-based alloys have good bio-compatibility and low Young's modulus, which are considered as a great potential for biomedical applications [7−9]. Fundamental information is very helpful for the design of novel Ti−Nb−Zr-based alloys, and the investigations on the Young's modulus, hardness, and diffusion coefficients of the Ti-rich Ti−Nb−Zr−(Cr, Hf, Mo, and Ta) quaternary alloys have been reported in the literature [9−13].

Corresponding author: Wei-min CHEN, E-mail: chenweiming126@jnu.edu.cn, chenweiming126@163.com
DOI: 10.1016/S1003-6326(23)66287-9

However, there is no systematic study on the effect of W on the elasto-plastic and diffusion properties of BCC Ti−Nb−Zr-based alloys to date. Therefore, more explorations to understand several elasto-plastic and diffusion property data of the W-containing Ti−Nb−Zr-based alloys are strongly necessary.

Depth-sensing instrumented indentation is widely used for many material systems to extract elasto-plastic properties from the load (P) of the indenter tip and displacement (h) of the tip into the materials [14]. The well-known Oliver−Pharr analysis method [15] has been embedded into operating system to determine the basic properties (Young's modulus (E) and hardness (H)). In addition, reverse analysis algorithm [16], which is based on the step-by-step analytical method [17], can be directly utilized to obtain the elasto-plastic properties which include modulus, hardness, representative stress ($\sigma_{0.033}$, $\sigma_{0.082}$, or even yield strength), and strain hardening coefficient (n). Nanoindentation on the specimens with the composition gradient (diffusion couples or multiples) is used as a high-throughput method to determine the composition-dependent elasto-plastic property data. Very recently, machine learning (ML) method has been utilized to predict the Young's modulus and hardness of multicomponent alloys [18,19]. Interdiffusion coefficient in the materials represents the influence of concentration gradient of one solute element on the diffusion rate of one solute element in the presence of a solvent element, which can be determined from composition profile of the diffusion couple [20].

The objective of this work is to explore the elasto-plastic and diffusion properties of BCC Ti−Nb−Zr−W alloys within a wide range of composition. Firstly, six diffusion couples of Ti−Nb−Zr−W system were annealed at 1273 K. Then, nanoindentation tests and electron probe microanalysis (EPMA) were conducted on the diffusion couples to obtain the elasto-plastic properties and compositions, respectively. Then, the composition-dependent databanks on elasto-plastic properties and interdiffusion coefficients of BCC Ti−Nb−Zr−W system were respectively developed by the ML and pragmatic numerical inverse methods, which were used to analyze the processability of Ti-rich Ti–Nb–Zr–W alloys during the hot working. Finally, wear resistance of refractory multi-element alloys was discussed and verified by the wear experiments.

2 Experimental

2.1 Material preparation and characterization

Ti (purity: 99.999%), Nb (purity: 99.95%), W (purity: 99.95%), and Zr (purity: 99.9%) slugs were used in this experiment. The Ti-rich ternary alloys remelted by arc melting under an Ar atmosphere using a non-reactive W electrode (WKDHL−1, Opto-electronics Co., Ltd., Beijing, China) were cut into blocks, and then homogenized in vacuum condition at (1273±2) K for 7 d in an ELF1106 type furnace (Carbolite Gero Co., Ltd., United Kingdom). The crystalline phase of the heat-treated blocks was identified by X-ray diffraction (XRD) using an Ultima IV diffractometer (Rigaku, Tokyo, Japan) with monochromatic Cu K_α radiation, which is presented in Fig. 1. The XRD patterns indicated that the samples prepared after annealing at 1273 K for 7 d were composed of a single BCC phase. And a Schottky field emission scanning electron microscope (FE-SEM, JSM-IT800, JEOL, Japan) equipped with an electron backscatter diffraction (EBSD) unit was used to observe grain size and texture. After that, the ground blocks with any two components were bound by Mo clamps, and annealed in vacuum condition at (1273±2) K for 25 h. After the vacuum annealing and quenching in the flowing water, the quaternary Ti−Nb−Zr−W diffusion couples were obtained. Cross-sections of the diffusion couples were ground and polished by SiC papers and diamond pastes, respectively. Compositions of six quaternary Ti−Nb−Zr−W diffusion couples were determined by EPMA (JXA−8530, JEOL, Japan), and the corresponding end-members are listed in Table 1. Young's moduli and hardness were obtained by the nanoindenter (Keysight G200, Agilent Technology, USA) according to Oliver−Pharr analysis [15]. The corresponding energy as shown in Fig. 2 was obtained from the load−displacement curve, which can be adopted for the calculation of elastic recovery. Moreover, reverse analysis algorithm proposed by DAO et al [16] was also utilized for the Young's modulus, hardness, and stress.

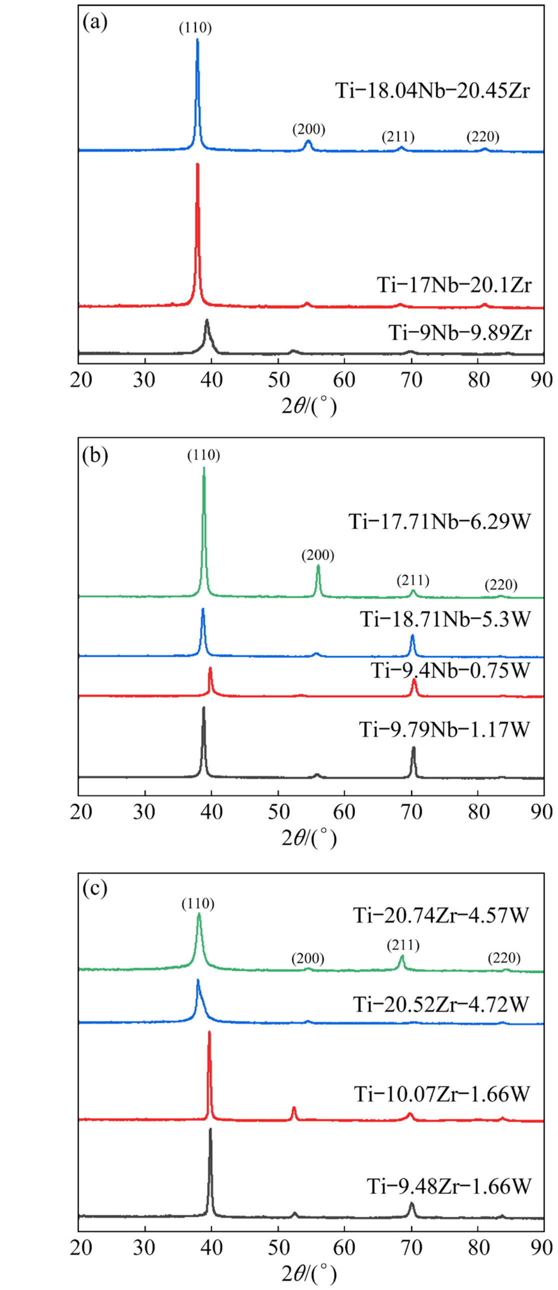

Fig. 1 XRD patterns of heat-treated Ti−Nb−Zr (a), Ti−Nb−W (b), and Ti−Zr−W (c) alloys in Ti−Nb−Zr−W system after annealing at 1273 K for 7 d

Table 1 Alloy compositions (%) in Ti−Nb−Zr−W diffusion couples

Couple No.	Composition
1	Ti−9Nb−9.89Zr/Ti−9.79Nb−1.17W
2	Ti−9.4Nb−0.75W/Ti−9.48Zr−1.66W
3	Ti−10.07Zr−1.66W/Ti−9Nb−9.89Zr
4	Ti−17Nb−20.17Zr/Ti−18.7Nb−5.3W
5	Ti−17.71Nb−6.29W/Ti−20.52Zr−4.72W
6	Ti−20.74Zr−4.57W/Ti−18.04Nb−20.45Zr

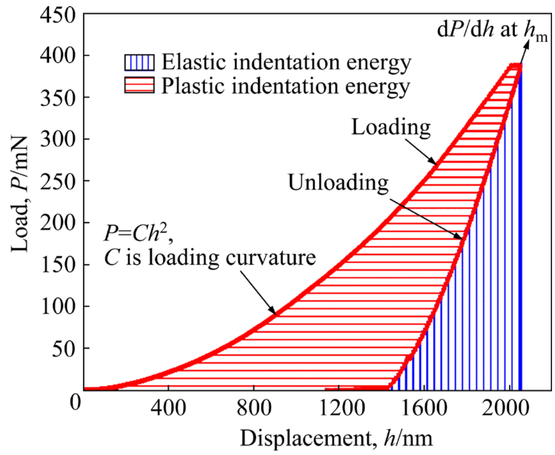

Fig. 2 Schematic diagram of loading and unloading in a cycle of indentation and corresponding energy fractions

In addition, four alloys including Ti−12.5%Nb−9.5%Zr−5.7%W, Ti−3%Nb−6%Zr−1.4%W, Ti−11%Nb−8.5%Zr−4%Sn, and Ti−18.7%Nb−12.8%Zr−3.5%Hf (mole fraction) were prepared by using arc melting and marked as TW6, TW1, TS, and TH, respectively. Several blocks with the size of 10 m × 10 m × 5 mm were homogenized in vacuum condition at (1273±2) K for 2 h, and then quenched in flowing water. The polished blocks in the as-cast (AC) and solution-treated (ST) states were tested on the reciprocating tribology tester (MFT−5000, Rtec-Instruments Multi-Functional Tribometer Co., Ltd., USA) combined with a zirconia ball (5 mm in diameter) as the friction pair. The detailed parameters for the experiments performed under an atmospheric atmosphere were a load of 2 N, time of 1 h, and frequency of 1 Hz. Friction coefficient of the sample was automatically generated during the experiment. And wear rate (Q) was calculated from the ratio of wear volume loss to sliding distance.

2.2 Prediction of Young's modulus and hardness

ML approach has been increasingly used to discover the correlations between compositions and properties including Young's modulus and hardness [21,22]. In this work, the measured alloy compositions in the above diffusion couples were denoted as input variables, while the Young's moduli or hardness were denoted as response variables. Cross validation method was used to randomly divide the input data into training and testing data without repeats. Gaussian processes regression (GPR), support vector regression (SVR), and linear regression (LR) models were employed to establish the ML prediction. Measured Young's moduli and hardness of 232 compositions were used as training and testing data.

2.3 Determination of interdiffusion coefficients

A pragmatic numerical inverse method based on Fick's second law was proposed to determine the composition-dependent interdiffusion coefficients in binary and multicomponent systems [23,24]. Calculations of composition-dependent interdiffusion coefficients of Ti-rich Ti−Nb−Zr−W system can be conducted by using a free accessible code called High-throughput Determination of Interdiffusion Coefficients (HitDIC) [25]. In this work, the thermodynamic parameters presented in Refs. [26,27] and an ideal solid solution model were utilized, and the mobility parameters reported in Refs. [28−31] were also used.

3 Results

Considering that all the end-members of diffusion couples are within a single BCC phase region of Ti−Nb−Zr−W system, Ti−18.7%Nb−5.3%W alloy was selected as the typical one. EBSD maps of Ti−18.7%Nb−5.3%W alloy are presented in Fig. 3. The Ti−18.7%Nb−5.3%W alloy fabricated by arc-melting and solution treatment is polycrystalline, as shown in the maps including inverse pole figure (IPF) and pole figure. EBSD orientation map indicates that this alloy has a generally homogeneous microstructure with no abnormal grain growth or preferred grain orientation. After a long annealing time at 1273 K, Ti−Nb−W alloy has an average grain size larger than 300 μm, which is appropriate for the investigations of bulk diffusion without the obvious effect of grain boundary.

The measured composition variations in the Ti−Nb−Zr−W diffusion couples have been presented in Fig. S1 in Supplementary Materials (SM). It can be seen from Fig. S1 that the measured composition profiles of Ti, Nb, Zr, and W in the BCC Ti−Nb−Zr−W diffusion couples can be well reproduced by the fitted data. Therefore, the fitted composition profiles are used to determine the compositions of the indentations, which can provide smooth and continuous data. The experimental elasto-plastic property data (i.e., Young's modulus, hardness, and elastic recovery) of the Ti−Nb−Zr−W alloys have been obtained from Oliver−Pharr method and presented in Fig. S2 in SM. As shown in Fig. S2, the variations of the experimental Young's moduli, hardness, and elastic recovery of the Ti alloys in the BCC Ti−Nb−Zr−W diffusion couples are within the range of 59−100 GPa, 2.5−5.2 GPa, and 0.20−0.36, respectively. Contact boundary of the diffusion couple is utilized as the reference position to correlate the fitted composition versus position with the nano-indentation results versus position. And then, elasto-plastic properties corresponding to the alloy composition variations can be obtained. Figure 4 shows the composition-dependent Young's modulus, hardness, and elastic recovery of BCC ternary and quaternary Ti-based alloys in the Ti−Nb−Zr−W diffusion couples. In Figs. 4(a−c), the experimental Young's moduli of the BCC Ti alloys slowly increase from the side of Ti−9%Nb−10%Zr to that of Ti−10%Nb−1%W, and then rapidly increase to that on the side of Ti−%10Zr−1.6%W. The experimental hardness and elastic recovery of the BCC Ti alloys in the diffusion couples of Ti−9.0%Nb−9.9%Zr/Ti−9.8%Nb−1.2%W and Ti−9.4%Nb−0.75%W/Ti−9.5%Zr−1.7%W have a similar trend. Since the elastic recovery of the Ti−10%Zr−1.6%W alloy is lower than that of the

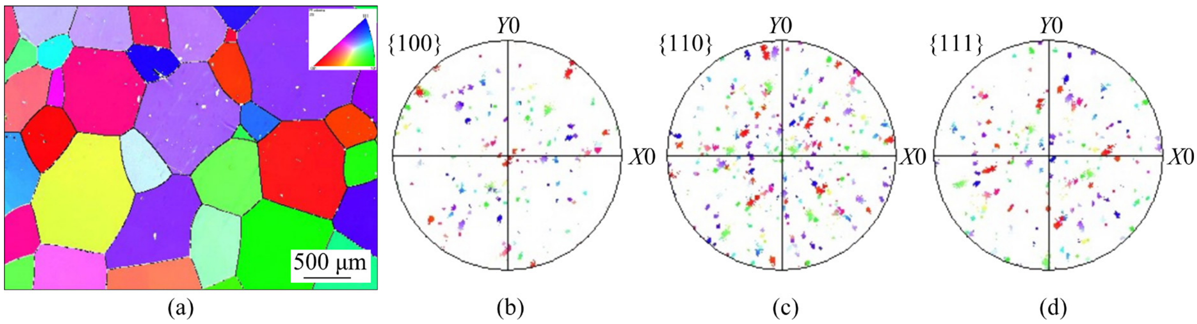

Fig. 3 Inverse pole (a) and pole figures (b−d) of Ti−18.7%Nb−5.3%W alloy after annealing at 1273 K for 7 d obtained from EBSD measurement

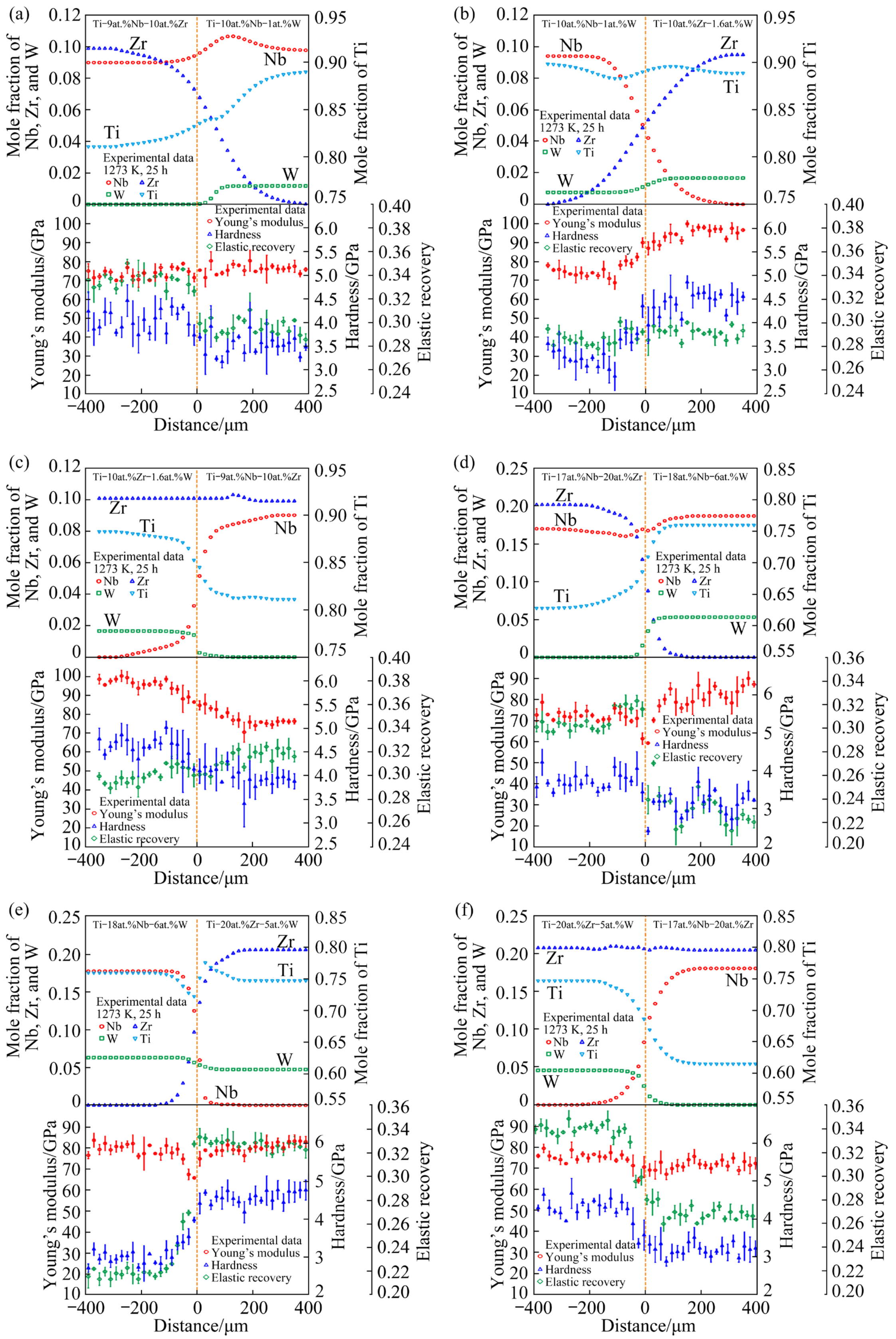

Fig. 4 Experimental Young's modulus, hardness, and elastic recovery of BCC Ti alloys in Ti−9.0%Nb−9.9%Zr/Ti−9.8%Nb−1.2%W (a), Ti−9.4%Nb−0.75%W/Ti−9.5%Zr−1.7%W (b), Ti−10.1%Zr−1.7%W/Ti− 9.0%Nb−9.9%Zr (c), Ti−17.0%Nb−20.2%Zr/Ti−18.7%Nb−5.3%W (d), Ti−17.7%Nb−6.3%W/Ti−20.5%Zr−4.7%W (e), and Ti−20.7%Zr−4.6%W/Ti−18.0%Nb−20.4%Zr (f) diffusion couples annealed at 1273 K for 25 h based on Oliver−Pharr method

Ti−9%Nb−10%Zr alloy, the elastic recovery on the side of Ti−10%Zr−1.6%W slowly increases to that on the Ti−9%Nb−10%Zr side. Moreover, there is the inverse relationship between the experimental hardness variations in the diffusion couples and the Nb concentration. It can be seen from Figs. 4(d−f) that the measured Young's moduli on the Ti−17%Nb−20%Zr side increase to those on the Ti−18%Nb−6%W and Ti−20%Zr−5%W sides, and the experimental Young's moduli of the quaternary alloys between the composition range of Ti−18%Nb−6%W and Ti−20%Zr−5%W have a sudden change. A minimum value of Young's modulus for the quaternary alloy exists in the above sudden change. The variation trend of the hardness in the Ti−17.0%Nb−20.2%Zr/Ti−18.7%Nb−5.3%W, Ti−17.7%Nb−6.3%W/Ti−20.5%Zr−4.7%W, and Ti−20.7%Zr−4.6%W/Ti−18.0%Nb−20.4%Zr diffusion couples is similar to that of the elastic recovery. Moreover, the experimental Young's modulus varies with the Ti concentration, while the variations of the experimental hardness and elastic recovery are inversely related to the Nb concentration. It is found that the addition of W can enhance the hardness of Ti−Zr alloys while the addition of W has a less effect on the elasto-plastic property of Ti−Nb alloys than that of Zr.

The reverse analysis algorithm [16] can provide elasto-plastic properties from the experimental load−depth curves by using a step-by-step method. Figure 5 shows the comparisons between the results of reverse analysis algorithm and the data of Oliver−Pharr method. In this figure, the Young's moduli and hardness obtained from Oliver−Pharr method are 7.05% and 11.58% higher than those of reverse analysis algorithm, respectively. The results obtained from two methods are close to each other, indicating that the two methods including Oliver−Pharr method and reverse analysis algorithm can be used to determine the reliable Young's modulus and hardness values. The relationship among the Young's modulus, hardness, and stress of reverse analysis algorithms for the BCC Ti−Nb−Zr−W system is presented in Fig. 6. Here, the stress corresponding to strain which is equal to 0.082 is within the range of 0.86−1.82 GPa. Moreover, hardness is 2.44 times stress when representative strain is 0.082. In addition, the stress when strain is 0.033 and strain hardening exponent of the BCC Ti−Nb−Zr−W system can be obtained

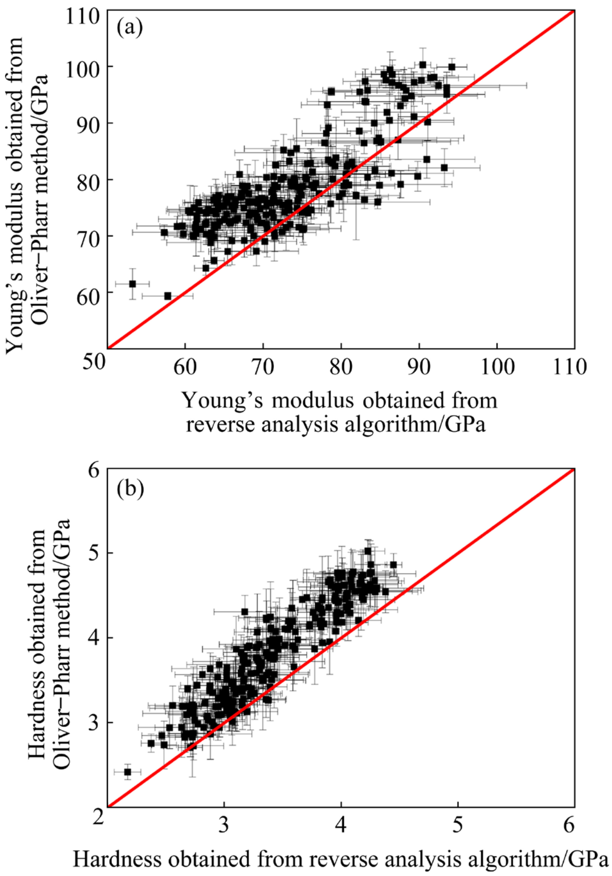

Fig. 5 Comparisons between experimental results of Oliver−Pharr method and data obtained from reverse analysis algorithm in Ti−Nb−Zr−W diffusion couples: (a) Young's modulus; (b) Hardness

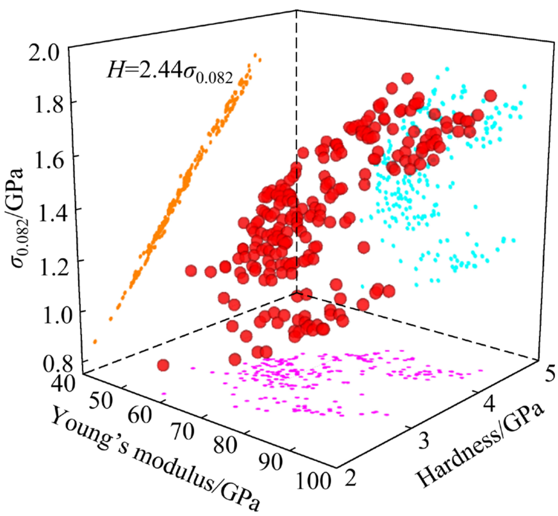

Fig. 6 Elasto-plastic property relationship of BCC Ti−Nb−Zr−W alloys based on reverse analysis algorithm

and shown in Fig. S3 in SM. In Fig. S3, the stress when strain is 0.033 has a large fluctuation (1.1−3.5 GPa) while the strain hardening exponent of BCC Ti−Nb−Zr−W system slightly fluctuates up and down near 0.2 (0.16−0.24). Moreover, the point projections of the measured data into a two-dimensional stress−hardness drawing (solid circles in orange color) in Fig. 6 show that there is a linear relationship between hardness and stress and the ratio of hardness to stress is 2.44.

The Young's modulus and hardness databanks of the Ti−Nb−Zr−W system are developed by using ML approach based on the measured data (232 data points). The root mean-squares error (RMSE) and the coefficient of determination (R^2) for GPR, SVR, and LR models are listed in Table 2. It can be seen from Table 2 that GPR model has the lowest RMSE and the highest R^2. The results indicate that this model has the high prediction accuracy for the calculations of Young's modulus and hardness in the Ti−Nb−Zr−W system. Thus, the Young's modulus and hardness corresponding to the measured alloy compositions can be predicted from the present databank based on GPR model, which are presented in Fig. 7, showing that the predicted Young's moduli and hardness are consistent with the measured data, indicating the accuracy of the present ML databank in a certain composition space. The Young's moduli predicted from ML databank are used in the subsequent calculations. The predictions of ML method are evaluated from the given data without the prior assumption. However, their validity strongly depends on the composition range of the given Young's modulus and hardness.

Table 2 RMSE and R^2 of GPR, SVR, and LR models for Young's modulus and hardness in Ti−Nb−Zr−W system

Property	GPR		SVR		LR	
	RMSE/GPa	R^2	RMSE/GPa	R^2	RMSE/GPa	R^2
Young's modulus	2.69	0.89	3.23	0.85	2.99	0.87
Hardness	0.23	0.84	0.24	0.83	0.26	0.81

In the determination of interdiffusion coefficients, both the thermodynamic parameters and ideal solid solution model are utilized here to provide the thermodynamic factors. Thus, the interdiffusion coefficients with and without the consideration of thermodynamic parameters can be obtained and accompanied with two sets of the model-predicted composition profiles. Figure S4

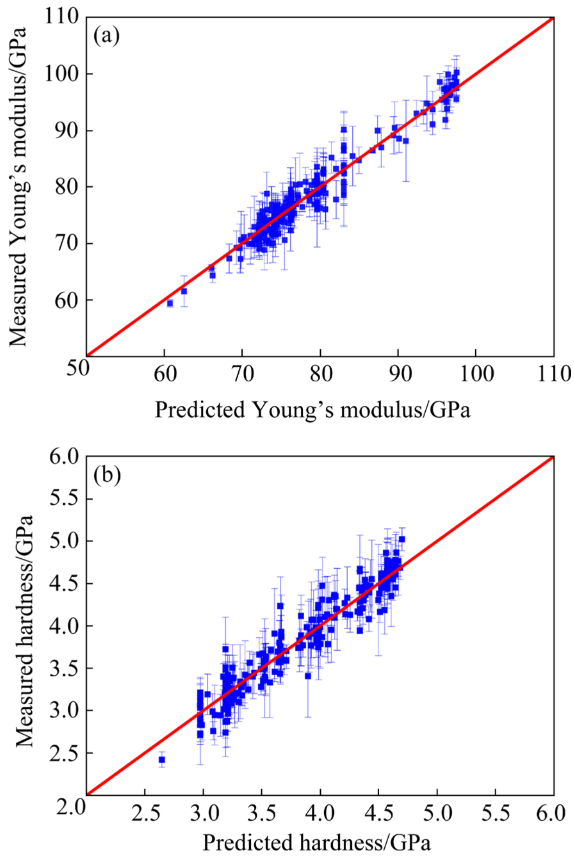

Fig. 7 Comparison between measured Young's modulus (a) and hardness (b) of Ti−Nb−Zr−W alloys and predicted data by using ML method

in SM shows the comparison between six sets of model-predicted composition profiles of Ti−Nb−Zr−W diffusion couples at 1273 K and the measured data. It can be seen from the figure that the model-predicted composition profiles in the assumption of an ideal solid solution model (solid lines) agree better with the experimental profiles than those with the consideration of thermodynamic parameters (dash lines). Several singular turning points of the simulated composition profiles are caused by the thermodynamic parameters, indicating that the thermodynamic parameters of BCC Ti−Nb−Zr−W system need to be modified according to the present diffusion information. Therefore, the results of an ideal solid solution model are determined here as the interdiffusion coefficients of Ti-rich Ti−Nb−Zr−W system at 1273 K, and demonstrated by the color variations in the composition space of a quaternary system. The main interdiffusion coefficients obtained by using pragmatic numerical inverse method are shown in Fig. 8. The interdiffusion coefficients obviously vary with the compositions of three solute elements Nb, Zr, and W. Moreover, three main interdiffusion coefficients including $\tilde{D}^{\mathrm{Ti}}_{\mathrm{WW}}$, $\tilde{D}^{\mathrm{Ti}}_{\mathrm{NbNb}}$, and $\tilde{D}^{\mathrm{Ti}}_{\mathrm{ZrZr}}$ are all positive, and the values of $\tilde{D}^{\mathrm{Ti}}_{\mathrm{ZrZr}}$ and $\tilde{D}^{\mathrm{Ti}}_{\mathrm{WW}}$ are the largest and the lowest, respectively.

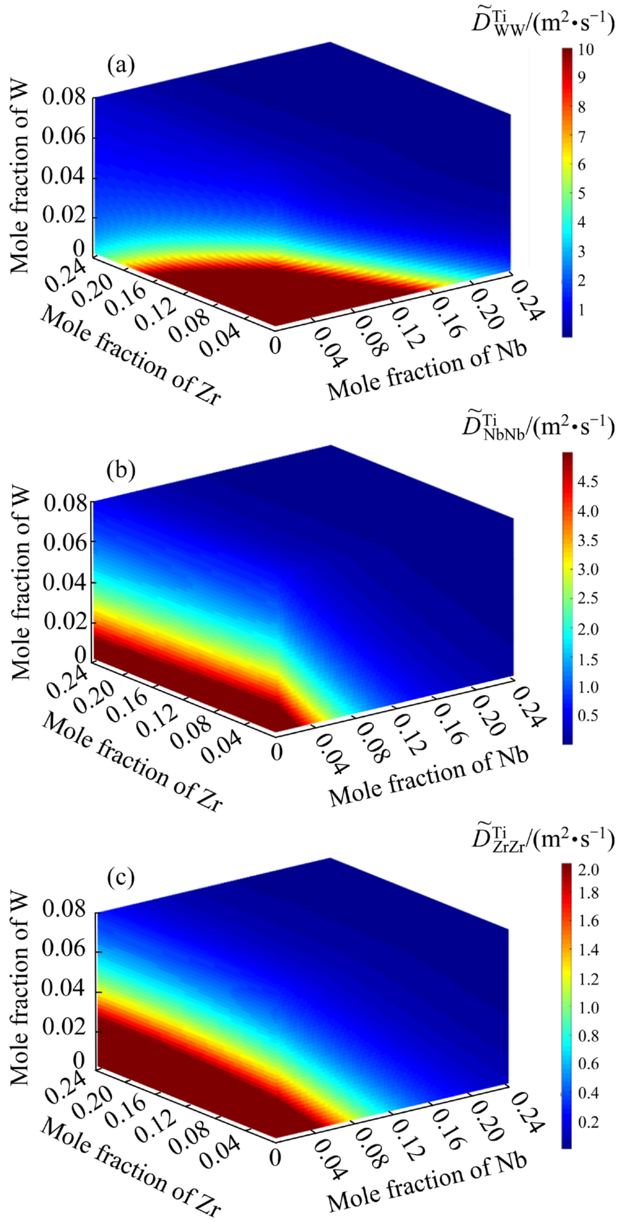

Fig. 8 Main interdiffusion coefficients $\tilde{D}^{\mathrm{Ti}}_{\mathrm{WW}}$ (a), $\tilde{D}^{\mathrm{Ti}}_{\mathrm{NbNb}}$ (b), and $\tilde{D}^{\mathrm{Ti}}_{\mathrm{ZrZr}}$ (c) of Ti-rich Ti−Nb−Zr−W system at 1273 K determined by using pragmatic numerical inverse method

Diffusive creep and superplasticity are very important for the production and applications in aerospace, biomedical, and automotive sectors [32,33]. The deformation rate, which is considered a regime of high temperature creep or superplasticity, is expressed in terms of steady state strain $\dot{\varepsilon}$ [34,35]. For diffusion-controlled processes, the steady state strain rate can be expressed in explicit form as [36−38]

$$\dot{\varepsilon}=\frac{FD\sigma^{q}}{E^{m}} \tag{1}$$

where F is an interaction constant, D is the diffusivity, σ is the stress, E is the Young's modulus, and exponents q and m are the values which are equal to or larger than 3. For simplicity, the Young's modulus at intermediate temperature is assumed to be linearly related with that at room temperature, which is in good agreement with the linear relationship between modulus and temperature utilized in Ref. [38]. Moreover, based on the comprehensive comparisons between steady state creep characteristics and lattice diffusion characteristics [35], the effective diffusivity D_{eff} is related to the main interdiffusion coefficient of the solute element with large atomic radius. Therefore, a hot workability parameter is defined here by ratio of main interdiffusion coefficient of large solute to cube of Young's modulus, which is tightly related to the behaviors during the hot working. By using a combination of the ML-type Young's modulus databank and interdiffusion coefficients determined via the pragmatic numerical inverse method at 1273 K, hot workability parameter D_{eff}/E^3 at each composition point of Ti-rich Ti−Nb−Zr−W system can be obtained. Figure 9 shows the variations of D_{eff}/E^3 for the Ti-rich Ti−Nb−Zr−W alloys. It should be noted that the values of effective diffusivity D_{eff} are the interdiffusion coefficients $\tilde{D}^{\mathrm{Ti}}_{\mathrm{WW}}$, $\tilde{D}^{\mathrm{Ti}}_{\mathrm{NbNb}}$, and $\tilde{D}^{\mathrm{Ti}}_{\mathrm{ZrZr}}$ for BCC Ti−W, Ti−Nb(−W), and Ti−Zr(−Nb−W) alloys at 1273 K, which is caused by the atomic radii of three solute elements W, Nb, and Zr. In Fig. 9, the D_{eff}/E^3 value of the Ti−Nb−Zr−W alloys ranges from 8.8×10^{-22} to 3.2×10^{-19} m²/(s·GPa). The results indicate that the hot workability parameter strongly depends on the composition variations. The D_{eff}/E^3 value decreases with the increasing content of solute elements W and Nb, which can enhance the Young's modulus and slow the diffusion rate. It also indicates that the W content should be controlled in the aspect of the nice processability. However, the refractory multi-element alloys with the low hot workability parameter may have good high temperature creep resistance. The addition of element Zr is helpful for improving the processability of Ti

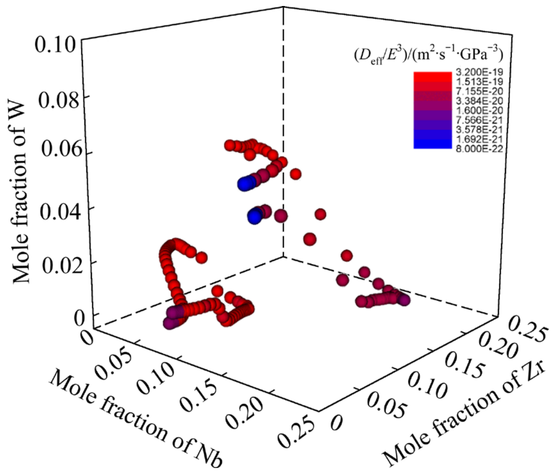

Fig. 9 Variations of D_{eff}/E^3 in Ti-rich Ti−Nb−Zr−W system (In this work, the values of D_{eff} for BCC Ti−W, Ti−Nb(−W), and Ti−Zr(−Nb−W) alloys are the interdiffusion coefficients $\tilde{D}^{\text{Ti}}_{\text{WW}}$, $\tilde{D}^{\text{Ti}}_{\text{NbNb}}$, and $\tilde{D}^{\text{Ti}}_{\text{ZrZr}}$ at 1273 K, respectively)

alloys during the hot working. In addition, according to the diffusion mobility descriptions [39] and experimental Young's modulus data [40], a value of 7.25×10^{-20} $\text{m}^2/(\text{s}\cdot\text{GPa}^3)$ is acquired as the hot service parameter of Ti−6Al−4V alloy, which can be used for comparisons in terms of processability. The hot service parameter of Ti alloys is larger than 7.25×10^{-20} $\text{m}^2/(\text{s}\cdot\text{GPa}^3)$, which may indicate that Ti alloys have nice processability at intermediate temperatures. Based on the experimental elasto-plastic properties and the calculated hot workability parameters, Ti−(2.5−3.5)%Nb−(5.5−6.5)%Zr−(1.2−1.6)%W alloy has the specific Young's modulus ((88.5−90.5) GPa), high hardness ((4.1−4.3) GPa), reasonable elastic recovery (0.295±0.002), and high hot workability parameter $((2.4-2.7)\times10^{-19}$ $\text{m}^2/(\text{s}\cdot\text{GPa}^3))$, which satisfies the requirements of the artificial enamel and can be utilized as promising alloy with optimum integrated properties for dental applications. It is also found that Ti−12.5%Nb−9.6%Zr−5.6%W alloy has low Young's modulus of (64±1) GPa, relatively high hardness of (3.4±0.1) GPa, and hot workability parameter of $(1.3\pm0.1)\times10^{-19}$ $\text{m}^2/(\text{s}\cdot\text{GPa}^3)$, which is suitable for the development of bio-alloy with low modulus.

The high-throughput method used in the present work provides a huge amount of elasto-plastic and diffusion properties data from limited samples with minimal experimental efforts, and is very beneficial to substantially accelerating the design and development of bio-alloys with desired properties [41]. According to the previous investigations [8,13], Ti−11%Nb−8.5%Zr−4%Sn and Ti−18.7%Nb−12.8%Zr−3.5%Hf alloys were found to be potential Ti bio-alloys with nice mechanical properties. Ti−11%Nb−8.5%Zr−4%Sn alloy has a Young's modulus of (53±3) GPa and hardness of (3.1±0.3) GPa, while Ti−18.7%Nb−12.8%Zr−3.5%Hf has a Young's modulus of (61±4) GPa and a hardness of (3.2±0.2) GPa. Therefore, four Ti−Nb−Zr-based alloys including Ti−12.5%Nb−9.6%Zr−5.6%W, Ti−3%Nb−6%Zr−1.4%W, Ti−11%Nb−8.5%Zr−4%Sn, and Ti−18.7%Nb−12.8%Zr−3.5%Hf are selected and prepared for the subsequent wear tests. Figure 10(a) shows the friction coefficients of the Ti−Nb−Zr−W (TW1 and TW6), Ti−Nb−Zr−Sn (TS), and Ti−Nb−Zr−Hf (TH) alloys. The friction coefficients of the solution-treated alloys are slightly lower than those of the arc-melted alloys. Arc-melted Ti−Nb−Zr−Sn alloy has the maximum friction coefficient, and the friction coefficient of ST Ti−Nb−Zr−Hf alloy is higher than those of Ti−Nb−Zr−W and Ti−Nb−Zr−Sn alloys after the solution annealing. The wear rates of the Ti−Nb−Zr−W, Ti−Nb−Zr−Sn, and Ti−Nb−Zr−Hf alloys are presented in Fig. 10(b). In Fig. 10(b), the wear rate of the solution-treated alloys is lower than that of the arc-melted alloys, which indicates that the wear property can be significantly improved by the short solution annealing. TS and TW6 alloys have the highest and lowest wear rate, respectively. The low wear rate of TW6 alloy may be related to the high W content. The wear rate of AC TW6 alloy is slightly higher than that of Ti−Zr−Nb−Ta−Mo high entropy alloys, but the result of ST TW6 alloy is lower than the literature data [42]. The experimental wear volume of Ti−Nb−Zr-based alloys is illustrated in Fig. S5 in SM, and is similar to the variations of wear rate. The two-dimensional cross-sections of AC and ST Ti−Nb−Zr-based alloys after the wear tests are presented in Figs. 10(c, d), respectively. It is seen from Figs. 10(c, d) that AC TS alloy has the largest grinding width and depth, while ST TW6 alloy has the smallest grinding width and depth. The cross-sections also display that TW6 alloy after the solution treatment has an excellent wear property.

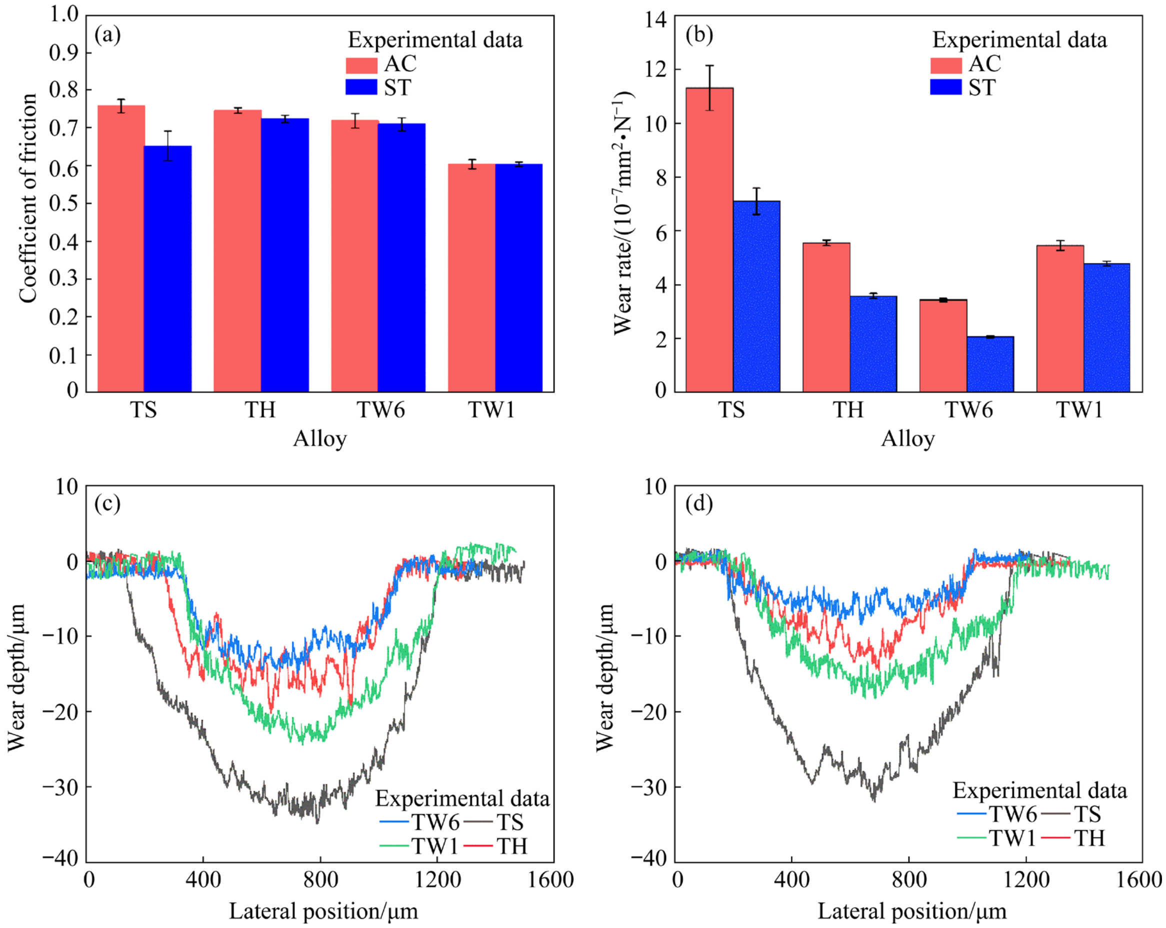

Fig. 10 Coefficient of friction (a), wear rate (b), and two-dimensional cross-sections of AC (c) and ST (d) Ti−Nb−Zr-based quaternary alloys after wear tests

4 Discussion

Considering the fact that Young's modulus is directly proportional relationship with bulk modulus and bulk modulus is in negative correlation with equilibrium lattice constant (or equilibrium volume), equilibrium lattice constant can be reflected by the Young's modulus, namely, the higher the Young's modulus, the lower the equilibrium lattice constant. Thus, the variation trend of the equilibrium lattice constant in the BCC Ti−Nb−Zr−W system can be obtained from Fig. 7(a). The equilibrium lattice constant of binary Ti alloy increases with increasing the Nb or Zr content, but decreases with increasing the W content. The result is consistent with the effect of atomic radii of solutes. The variation of equilibrium lattice constant for multicomponent Ti alloys in the Ti−Nb−Zr−W system is complex due to the mutual influence of solute elements Nb, Zr, and W. Thus, empirical parameter, for example, atomic size difference, can be utilized for the design of BCC Ti alloys. The similar work has been performed in Ref. [43], which refers to the design basis of high entropy or multi-principal element alloys.

It can be seen from the dimensionless functions that the stress when strain is 0.033 is very sensitive to the loading curvature which ranges from 70 to 120 GPa, and the stress when strain is 0.082 is less sensitive to the experimental scatter. Therefore, stress when strain is 0.082 can be considered as a representative stress for the BCC Ti−Nb−Zr−W system. The step-by-step procedure is used in the calculations of reverse analysis algorithm to construct the elasto-plastic parameters. It is noted that the required elasto-plastic property parameters including the Young's modulus and stress when strain is 0.082 are achieved with the aid of limited amount of experimental indentation information, which are accurate and suitable for comparing with the results of tensile tests.

Generally, the materials which have high wear resistance can be used for a long service time [44]. Wear resistance can be indirectly explored by using the hardness to elastic modulus ratios (H/E and H^3/E^2). Here, these two ratios are calculated with the experimental Young's moduli and hardness to evaluate the wear resistance of the BCC-Ti alloys. In Ref. [11], the values 0.04 and 0.009 are recommended as the reference data of H/E and H^3/E^2 for comparisons, respectively, which are also used in this study. According to statistical analysis of the results for 232 composition points, the H/E value of 204 composition points is larger than or equal to 0.04. And at these points, the H^3/E^2 value of 132 points is larger than or equal to 0.009 GPa. The result indicates that the Ti−Nb−Zr−W alloys have relatively high wear resistance, which can be used for bio-applications (i.e., orthopedic and dental applications). Actually, the above analysis is also supported by the Young's modulus and hardness data obtained from reverse analysis algorithm. The friction coefficient reflects the lubrication effect of the materials, and there is no direct correlation between friction coefficient and wear property [42,45]. However, the wear property of the materials is generally determined by the wear rate. The relationship between wear rate and indirect wear resistance parameter (H/E and H^3/E^2) has been plotted in Fig. 11. It is found that the higher the indirect wear resistance parameter is, the lower wear rate is. TW1 alloy has higher hardness value and lower indirect wear resistance parameter, and thus the wear rate of TW1 alloy is greater than that of TW6 alloy. Hardness has an important effect on the wear property, but the combination of hardness and Young's modulus is more successful to be a indicator of wear property for Ti alloys. The TS alloy has the high ratio of hardness to Young's modulus but the highest wear rate. The significant abrasive wear and fatigue spallation of TS alloy may be caused by frictional heating during the dry sliding and the low frictional coefficient for the lubrication effect.

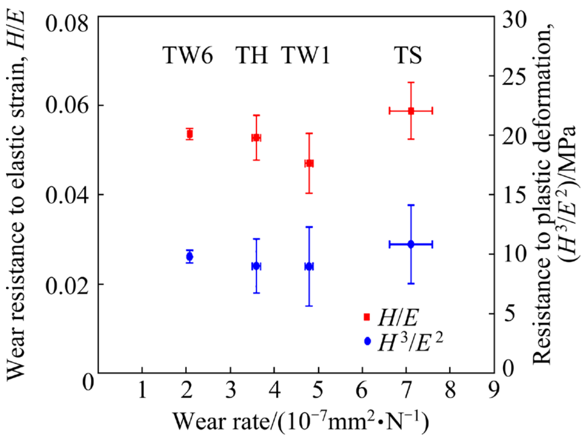

Fig. 11 Relationship between wear rate and indirect wear resistance parameter for Ti−Nb−Zr-based alloys

5 Conclusions

(1) The experimental Young's moduli, hardness, elastic recovery, and representative stress of the multicomponent Ti alloys are composition-dependent, which are within the range of 59−104 GPa, 2.3−5.2 GPa, 0.20−0.36, and 0.86−1.82 GPa, respectively. The elasto-plastic property and interdiffusion coefficient databanks of the BCC Ti−Nb−Zr−W system are respectively developed by using the ML and pragmatic numerical inverse methods and verified by comparing with the measured data.

(2) A plot of a hot workability parameter in the Ti−Nb−Zr−W system is shown, which indicates that the addition of element Zr improves the processability of Ti alloys during the hot working while the addition of element W lowers their processability. Moreover, Ti−12.5%Nb−9.6%Zr−5.6%W alloy is found to have the lowest wear rate during the dry sliding compared to the other three Ti−Nb−Zr-based quaternary alloys.

(3) The results indicate that the addition of W can enhance the wear resistance of Ti alloys, which is caused by the fact that solute element W can effectively improve the hardness of Ti−Nb−Zr-based alloys. This work reveals that Ti−Nb−Zr−W alloys have high hardness and good wear resistance, which are very suitable for bio-applications.

Acknowledgments

This work was financially supported by the National Natural Science Foundation for Youth of China (No. 51701083), the Guangzhou Science and Technology Association Young Talent Lifting Project, China (No. X20210201054), the Open Fund of National Joint Engineering Research Center for Abrasion Control and Molding of Metal Materials, China (No. HKDNM201903), and the National Key Research and Development Project, China (No. 2020YFC1107202).

Supplementary materials

The supplementary materials in this paper can be found at: http://tnmsc.csu.edu.cn/download/07-p2646-2022-0280-Supplementary_Materials.pdf.

References

[1] LEI Zhi-feng, LIU Xiong-jun, WU Yuan, WANG Hui, JIANG Suihe, WANG Shu-dao, HUI Xi-dong, WU Yi-dong, GAULT B, KONTIS P, RAABE D, GU Lin, ZHANG Qing-hua, CHEN Hou-wen, WANG Hong-tao, LIU Jia-bin, AN Ke, ZENG Qiao-shi, NIEH T G, LU Zhao-ping. Enhanced strength and ductility in a high-entropy alloy via ordered oxygen complexes [J]. Nature, 2018, 563: 546−550.

[2] XU Qin, CEHN De-zhi, WANG Cong-rui, CAO Wen-chao, WANG Qi, CUI Hong-zhi, ZHANG Shu-yan, CHEN Rui-run. Effects of La on microstructure and mechanical properties of $NbMoTiVSi_{0.2}$ refractory high entropy alloys [J]. Transactions of Nonferrous Metals Society of China, 2021, 31: 512−520.

[3] BAI Lin-hui, HU Yong-le, LIANG Xiu-bing, TONG Yong-gang, LIU Jian, ZHANG Zi-bing, LI Ye-jun, ZHANG Jian. Titanium alloying enhancement of mechanical properties of NbTaMoW refractory high-entropy alloy: First-principles and experiments perspective [J]. Journal of Alloys and Compounds, 2021, 857: 157542.

[4] LEONG Z, RAMAMURTY U, TAN T L. Microstructural and compositional design principles for Mo−V−Nb−Ti−Zr multi-principal element alloys: A high-throughput first-principles study [J]. Acta Materialia, 2021, 213: 116958.

[5] SENKOV O N, GILD J, BUTLER T M. Microstructure, mechanical properties and oxidation behavior of NbTaTi and NbTaZr refractory alloys [J]. Journal of Alloys and Compounds, 2021, 862: 158003.

[6] LIU Qing, WANG Guo-feng, SUI Xiao-chong, XU Ye, LIU Yong-kang, YANG Jian-lei. Ultra-fine grain Ti_xVNbMoTa refractory high-entropy alloys with superior mechanical properties fabricated by powder metallurgy [J]. Journal of Alloys and Compounds, 2021, 865: 158592.

[7] HUSSEIN M, ADESINA A Y, KUMAR M, AZEEM M, SOROUR A, AL-AQEELI N. Improvement of in vitro corrosion, wear, and mechanical properties of newly developed Ti alloy by thermal treatment for dental applications [J]. Transactions of Nonferrous Metals Society of China, 2021, 31: 952−966.

[8] WEN Zhu-hao, WANG Yao, CHEN Wei-min, ZHANG Li-jun, DU Yong. Investigation of mechanical and diffusion properties in bcc Ti−Nb−Zr−Sn alloys via a high-throughput method [J]. Transactions of Nonferrous Metals Society of China, 2021, 31: 3405−3415.

[9] LING Jin-feng, CHEN Wei-min, SHENG Yin-ying, LI Wei, ZHANG Li-jun, DU Yong. A MGI-oriented investigation of the Young's modulus and its application to the development of a novel Ti–Nb–Zr–Cr bio-alloy [J]. Materials Science and Engineering C, 2020, 106: 110265.

[10] CHEN Wei-min, LI Wei, DU Yong. Investigations on diffusion behaviors in Ti-rich Ti–Nb–Zr–Cr system: Experimental measurement and CALPHAD modeling [J]. Calphad, 2018, 62: 223−231.

[11] LING Jin-feng, HUANG Dan-dan, BAI K, LI Wei, YU Zhen-tao, CHEN Wei-min. High-throughput development and applications of the compositional mechanical property map of the β titanium alloys [J]. Journal of Materials Science & Technology, 2021, 71: 201−210.

[12] LING Jin-feng, WEN Zhu-hao, YANG Gui-ming, WANG Yao, CHEN Wei-min. A CALPHAD-type Young's modulus database of Ti-rich Ti−Nb−Zr−Mo system [J]. Calphad, 2021, 73: 102255.

[13] WEN Zhu-hao, WANG Yong-zhe, LING Jin-feng, CHEN Wei-min, ZHANG Li-jun, DU Yong. High-throughput determination of the composition-dependent mechanical and diffusion properties in β Ti−Nb−Zr−Hf refractory alloys [J]. Journal of Alloys and Compounds, 2021, 876: 160150.

[14] LU L, DAO M, KUMAR P, RAMAMURTY U, KARNIADAKIS G E, SURESH S. Extraction of mechanical properties of materials through deep learning from instrumented indentation [J]. Proceedings of the National Academy of Sciences of the United States of America, 2020, 117: 7052−7062.

[15] OLIVER W C, PHARR G M. An improved technique for determining hardness and elastic modulus using load and displacement sensing indentation experiments [J]. Journal of Materials Research, 1992, 7: 1564−1583.

[16] DAO M, CHOLLACOOP N, van VLIET K J, VENKATESH T A, SURESH S. Computational modeling of the forward and reverse problems in instrumented sharp indentation [J]. Acta Materialia, 2001, 49: 3899−3918.

[17] SURESH S, CIANNAKOPOLOS A E. A new method for estimating residual stresses by instrumented sharp indentation [J]. Acta Materialia, 1998, 46: 5755−5767.

[18] YANG Fei, LI Zhen, WANG Qing, JIANG Bei-bei, YAN Biao-jie, ZHANG Peng-cheng, XU Wei, DONG Chuang, LIAW P K. Cluster-formula-embedded machine learning for design of multicomponent β-Ti alloys with low Young's modulus [J]. NPJ Computational Materials, 2020, 6: 1−11.

[19] WEN Zhu-hao, HU Yun-long, CHEN Wei-min, ZHANG Qiang, ZHANG Li-jun, DU Yong. High-throughput exploration of the composition-dependent elasto-plastic properties in Co−Ni−W system [J]. Journal of Alloys and Compounds, 2022, 896: 163061.

[20] DIVYA V D, RAMAMURTY U, PAUL A. Interdiffusion and solid solution strengthening in Ni–Co–Pt and Ni–Co–Fe ternary systems [J]. Philosophical Magazine, 2013, 93: 2190−2206.

[21] ZOU C X, LI J S, WANG W Y, ZHANG Y, LIN D Y, YUAN R H, WANG X D, TANG B, WANG J, GAO X Y, KOU H C, HUI X D, ZENG X Q, QIAN M, SONG H F, LIU Z K, XU D S. Integrating data mining and machine learning to discover high-strength ductile titanium alloys [J]. Acta Materialia, 2021, 202: 211−221.

[22] QIAO L, LAI Z H, LIU Y, BAO A, ZHU J C. Modelling and prediction of hardness in multi-component alloys: A combined machine learning, first principles and experimental study [J]. Journal of Alloys and Compounds, 2021, 853: 156959.

[23] CHEN Wei-min, ZHANG Li-jun, DU Yong, TANG Cheng-ying, HUANG Bai-yun. A pragmatic method to determine the composition-dependent interdiffusivities in ternary systems by using a single diffusion couple [J]. Scripta Materialia, 2014, 90/91: 53−56.

[24] CHEN Wei-min, ZHONG Jing, ZHANG Li-jun. An augmented numerical inverse method for determining the composition–dependent interdiffusivities in alloy systems by using a single diffusion couple [J]. MRS Communications, 2016, 6: 295−300.

[25] ZHONG Jing, CHEN Wei-min, ZHANG Li-jun. HitDIC: A free-accessible code for high-throughput determination of interdiffusion coefficients in single solution phase [J]. Calphad, 2018, 60: 177−190.

[26] GUILLERMET A F. Thermodynamic analysis of the stable phases in the Zr−Nb system and calculation of the phase diagram [J]. Zeitschrift fur Metallkunde, 1991, 82: 478−487.

[27] HU Biao, QIU Cheng-liang, CUI Sen-lin, WANG Pei-sheng, ZHOU Jia-qiang, XU Wang-sheng, MIN Fan-fei, ZHAO Jing-rui. CALPHAD-type thermodynamic description of phase equilibria in the Ti−W−M (M=Zr, Mo, Nb) ternary systems [J]. The Journal of Chemical Thermodynamics, 2019, 131: 25−32.

[28] LIU Ya-jun, PAN Tong-yan, ZHANG Li-jun, YU Di, GE Yang. Kinetic modeling of diffusion mobilities in bcc Ti−Nb alloys [J]. Journal of Alloys and Compounds, 2009, 476: 429−435.

[29] LIU Ya-jun, ZHANG Li-jun, YU Di. Computational study of mobilities and diffusivities in bcc Ti−Zr and bcc Ti−Mo alloys [J]. Journal of Phase Equilibria and Diffusion, 2009, 30: 334−344.

[30] LIU Ya-jun, ZHANG Li-jun, PAN Tong-yan, YU Di, GE Yang. Study of diffusion mobilities of Nb and Zr in bcc Nb−Zr alloys [J]. Calphad, 2008, 32: 455−461.

[31] LIU Ya-jun, WANG Guan, WANG Jiang, KANG Zhi-tao. Mobilities and diffusivities for bcc Nb−W, Nb−Ta, Zr−Mo and Zr−Hf alloys [J]. Journal of Alloys and Compounds, 2013, 555: 381−389.

[32] LIU Yue, WU Jun-ming, WANG Zhi-chao, LU Xiao-gang, AVDEEV M, SHI Si-qi, WANG Chong-yu, YU Tao. Predicting creep rupture life of Ni-based single crystal superalloys using divide-and-conquer approach based machine learning [J]. Acta Materialia, 2020, 195: 454−467.

[33] ALABORT E, PUTMAN D, REED R C. Superplasticity in Ti−6Al−4V: Characterisation, modelling and applications [J]. Acta Materialia, 2015, 95: 428−442.

[34] LANGDON T G. A unified approach to grain boundary sliding in creep and superplasticity [J]. Acta Metallurgica et Materialia, 1994, 42: 2437−2443.

[35] MONMA K, SUTO H, OIKAWA H. Relation between High-temperature creep and diffusion in alloys (On the relation between high-temperature creep and diffusion in nickel-base solid solutions. VII) [J]. Journal of the Japan Institute of Metals and Materials, 1964, 28: 308−312.

[36] CANNON W R, SHERBY O D. High temperature creep behavior of class I and class II solid solution alloys [J]. Metallurgical Transactions, 1970, 1: 1030−1032.

[37] KASSNER M E, PÉREZ-PRADO M T. Five-power-law creep in single phase metals and alloys [J]. Progress in Materials Science, 2000, 45: 1−102.

[38] HE J Y, ZHU C, ZHOU D Q, LIU W H, NIEH T G, LU Z P. Steady state flow of the FeCoNiCrMn high entropy alloy at elevated temperatures [J]. Intermetallics, 2014, 55: 9−14.

[39] LINDWALL G, MOON K W, CHEN Z Q, MENGASON M, WILLIAMS M E, GORHAM J M, ZHAO J C, CAMPBELL C E. Diffusion in the Ti−Al−V system [J]. Journal of Phase Equilibria and Diffusion, 2018, 39: 731−746.

[40] HYNOWSKA A, PELLICER E, FORNELL J, GONZALEZ S, VAN STEENBERGE N, SURINACH S, GEBERT A, CALIN M, ECKERT J, BARO M D, SORT J. Nanostructured β-phase Ti−31.0Fe−9.0Sn and sub-μm structured Ti−39.3Nb−13.3Zr−10.7Ta alloys for biomedical applications: Microstructure benefits on the mechanical and corrosion performances [J]. Materials Science and Engineering C, 2012, 32: 2418−2425.

[41] LIN Hao-qin, LING Jin-feng, CHEN Wei-min, WANG Yao, WU Xiao-ke, ZHANG Li-jun. High-throughput determination of mechanical and diffusion properties in the Ti−Ta−Fe alloys [J]. Transactions of Nonferrous Metals Society of China, 2022, 32: 3963−3972.

[42] HUA Neng-bin, WANG Wen-jie, WANG Qian-ting, YE You-xiong, LIN Si-han, ZHANG Lei, GUO Qiao-hang, BRECHTIL J, LIAW P K. Mechanical, corrosion, and wear properties of biomedical Ti−Zr−Nb−Ta−Mo high entropy alloys [J]. Journal of Alloys and Compounds, 2021, 861: 157997.

[43] WANG C H, RUSSELL A M, CAO G H. A semi-empirical approach to the prediction of deformation behaviors of β-Ti alloys [J]. Scripta Materialia, 2019, 158: 62−65.

[44] XU Liu-jie, SONG Wan-li, MA Sheng-qiang, ZHOU Yu-cheng, PAN Kun-ming, WEI Shi-zhong. Effect of slippage rate on frictional wear behaviors of high-speed steel with dual-scale tungsten carbides (M_6C) under high-pressure sliding-rolling condition [J]. Tribology International, 2021, 154: 106719.

[45] HUA Neng-bin, CHEN Wen-zhe, WANG Qian-ting, GUO Qiao-hang, HUANG You-ting, ZHANG Tao. Tribocorrosion behaviors of a biodegradable $Mg_{65}Zn_{30}Ca_5$ bulk metallic glass for potential biomedical implant applications [J]. Journal of Alloys and Compounds, 2018, 745: 111−120.

难熔多组元 Ti−Nb−Zr−W 合金随成分变化弹塑性和扩散性能的高通量探索

闻祝浩[1]，林浩钦[1]，陈伟民[1]，Kewu BAI[2]，张利军[3]

1. 暨南大学 先进耐磨蚀及功能材料研究院，广州 510632；
2. Institute of High Performance Computing, Agency for Science, Technology and Research, Singapore 138632, Singapore；
3. 中南大学 粉末冶金国家重点实验室，长沙 410083

摘　要：组合材料合成和分析方法能够很好地描述 Ti−Nb−Zr−W 体系难熔多元合金的弹塑性和扩散特性。在 1273 K 温度固溶退火 25 h 后制备 6 组 Ti−Nb−Zr−W 四元扩散偶，并对其开展电子探针显微分析和纳米压痕测试。随后，采用 Oliver−Pharr 和反向分析算法等方法获得 Ti−Nb−Zr−W 体系宽广成分范围的随成分变化弹塑性。此外，采用机器学习和实用高效数值回归方法分别建立 Ti−Nb−Zr−W 体系体心立方相的弹塑性和互扩散系数数据库。同时，提出由杨氏模量与主互扩散系数之比所定义的热加工性能参数来评估热加工过程行为。最后，讨论难熔多元合金的耐磨性并进行实验验证。结果表明，低钨含量的富 Ti 难熔多元合金具有高硬度、良好的耐磨性、高应力和良好的热加工性能，而高钨含量并不能改善富 Ti 难熔合金的弹塑性。

关键词：弹塑性；互扩散系数；Ti−Nb−Zr−W 合金；扩散偶；纳米压痕

(Edited by Wei-ping CHEN)